IJAME

*Int. J. of Applied Mechanics and Engineering, 2023, vol.28, No.4, pp.94-113*
DOI: 10.59441/ijame/173021

# ROLE OF SUCTION/INJECTION ON ELECTROMAGNETOHYDRODYNAMIC NATURAL CONVECTION FLOW IN A POROUS MICROCHANNEL WITH ELECTROOSMOTIC EFFECT

Michael O. ONI* and Usman RILWAN
Department of Mathematics, Ahmadu Bello University, Zaria, NIGERIA
E-mail: michaeloni29@yahoo.com

In this paper we examined the role of suction/injection on time-dependent electromagnetohydrodynamic (EMHD) natural (free) convection flow in a vertical microchannel with electroosmotic effect. With the aid of the Laplace transformation method, the governing energy and momentum equations are converted from partial differential equations (PDEs into ordinary differential equations (ODEs) to obtain fluid temperature and velocity in the Laplace domain. The semi-analytical solutions of the velocity profile and temperature distribution have been derived using the Riemann sum approximation. Then a MATLAB program was written to study the effects of the Prandlt number *Pr*, Hartmann number *Ha*, electric field strength in the *x* and z directions respectively ($\bar{E}x$ and *Sz*) and the impact of the Grashof number *Gr* on fluid velocity, temperature, skin-friction and mass flow rate in terms of line graphs. The results show the role of suction/injection parameter altering the temperature distribution and velocity profile, and also how the governing parameters contribute to the flow formation.

**Key words:** EMHD, natural convection, suction/injection, electroosmotic flow.

## 1. Introduction

Magnetohydrodynamics (MHD) as one of the most important fields in fluid mechanics. It includes investigating how magnetic and electric forces affect the flow of electrically conducting liquids [1]. The Lorentz force-driven flow known as a magnetohydrodynamic flow is produced when an electrically conducting fluid interacts with a vertical magnetic field [2]. A few of the amazing advantages of the MHD micropump include pumping watery solutions, flow pumping, flow control, fluid mixing, thermal reactors, micro-coolers, forward and backward flow, chemical processes, ease of production, etc. [3]. MHD pump can be used in microfluidic devices due to its benefits over traditional pressure-driven flow and significant progress in the shrinking of fluidic systems, making it one of the most appealing study topics in microfluidic technology [4]. The MHD pump not only regulates flow and pumping, but also produces a complex secondary fluid with the help of mixing and string [5]. Numerous experimental, analytical, and computational research studies on MHD flow in microchannels have been described in the literature. Jang and Lee [2] found experimentally that the average flow rate increased when the magnetic field weakened. A microfluidic pump with an AC MHD propulsion mechanism was created by Lemoff and Lee [6]. Chakraborty and Paul [7] hypothetically investigated the combined effects of an MHD and elctroosmotic (EO) flow using parallel plate microchannels, in comparison to the scenario when magnetic effects are completely absent, they discovered that larger volumetric flow rates may be attained with a far lower electrical field. Sarkar and Ganguly [8] examined an MHD flow of nanofluids through a microchannel. They developed closed-form analytical equations for temperature distributions, Nusselt number, and velocity. In order to determine the perturbation solutions of the velocity and volume flow rate of the MHD EO flow with corrugated walls, Buren *et al.* [9] employed the perturbation expansion technique, which is characterized by a small amplitude periodic sinusoidal wave.

* To whom correspondence should be addressed

Moghaddam [10] carried out a numerical analysis of MHD micropumps using the power-law model. When the Hartmann number is less than a threshold value, shear-thinning fluids flow at a slower pace than Newtonian fluids. The opposite is true for shear-thinning fluids when the Hartmann number is greater than the critical threshold. In recent times, Xie and Jian [11] used the limited contrast technique to numerically examine pivoting MHD stream of power-law liquids through a limit microchannel.

Electroosmotic flow (EOF) is one of the powerful transportation methods which is activated by the application of an external electric field across a microchannel. Its future uses are extremely promising. As fluidic systems become gradually miniaturized, some of the most appealing study fields in microfluidic technology have been developed due to EOF's many advantages over a traditional pressure-driven flow and their potential uses in microfluidic devices [12]. The electric field produced by electroosmotic direct current (DC) causes the electroosmotic flow. The alternating current (AC) electric field is coupled to the time and frequency-dependent electroosmotic flow. Electroosmosis has a significant effect on fluid movement in the case of the AC electric field across the channels (Yang *et al.* [13] and Luo *et al.* [14]). Numerous attempts have been made to analyze the EOF of Newtonian and non-Newtonian fluid flows in parallel, circular, rectangular, and other irregularly shaped microchannels [15]. The impact of the buoyance force, wall asymmetric heat fluxes, and steady natural convection with electrokinetic effect in an electroosmotic flow was investigated by Oni and Jha [16]. Regardless of the size of the buoyance force, their conclusion demonstrates that the skin-friction and mass flow rate in the microchannel would have been overestimated by roughly 37% and *30%*, respectively, if the slip-condition at the microchannel walls had not been taken into account. In order to induce Joule heat with EOF, the accuracy and effectiveness of electrokinetic sample manipulation will be reduced [17, 18]. A time-dependent electroosmotic flow of viscoelastic fluids via a parallel plate microchannel with a constant pressure gradient and a vertical magnetic field was studied by Wang *et al.* [19]. In a rectangular cross-sectional 2D-channel, Yang and Kwok [20] and Kang *et al.* [21] created a pressure-driven flow and a time-dependent electrokinetic slippage flow to counterbalance the impacts of the electric double layer (EDL). Jayaraj *et al.* [22] made a flow analysis and mixing in various microchannel geometries. Many theoretical and practical experiments have been carried out in to examine the EOF in the presence of a magnetic field. The combined effects of an electric field and a magnetic field are expected to be particularly effective in transporting and controlling fluid samples in microfluidic devices. Chakraborty and Paul [23] studied the combined impacts of MHD and EO forces using a parallel plate microchannel and analyzed the impact of near-wall interaction potentials and the associated migrative fluxes on the flow. According to the studies, an electro-magneto-hydrodynamic (EMHD) effect paired with an EDL might improve the flow rate in microchannels. Jang and Lee [24] performed an experimental research with micropumps in a setting with a weak magnetic field to demonstrate that the flow rate rises significantly. Jian *et al.* [25] examined the effects of transient EMHD micropumps on two infinite parallel plates. The Lorentz force controls the flow for both the AC and DC EMHD pumps. The effects of electric and magnetic fields on the thermally developing mixed electroosmotic transport, pressure-driven nanofluid flow, viscous dissipation, and Joule heating in a microchannel were studied by Ganguly *et al.* [26] in a microchannel under the influence of electric and magnetic fields. They determined the velocity, temperature, and Nusselt number in the presence of the volume % of dispersed nanoparticles and particle agglomerations using the no-slip speed and no-jump temperature boundary conditions. Mirza *et al.* [27] theoretically investigated a transient electro-magnetohydrodynamic two-phase blood flow through a capillary tube. They considered the no-slip boundary condition, the pressure gradient, and the Joule heating effect with constant heat flow. Without minimizing the impacts of viscous dissipation, EDL, external electric and magnetic fields, or fluid flow via cylinder-shaped microchannels, their research established the thermal transport features of the fluid flow. When dealing with an externally applied magnetic field in a parallel plate microchannel, Tso and Sundaravadivelu [28] took into consideration the transverse electric field while neglecting EDL effects to study the impact of the electromagnetic field on the surface tension-driven flow. Duwairi and Abdullah [29] and Shit *et al.* [30] investigated the two-dimensional velocity and temperature distributions of an electro-magneto-hydrodynamic (EMHD) micropump. They considered thermal radiation, electromagnetic field-induced EDL effects, and Joule heating effects without viscous dissipation. Kiyasatfar and Pourmahmoud [31] studied the MHD non-Newtonian electroosmotic flow in a square microchannel in the presence of viscous dissipation and Joule heating effects using a computational

technique based on the finite difference method. Liu *et al.* [32] and Mondal *et al.* [33] analyzed the EMHD flow velocity and heat transfer in a curved rectangular microchannel in the presence of a vertical electric field and radial magnetic field. They confirmed that the temperature and velocity distributions have a significant impact on the pace of entropy creation. Sheikholeslami and Ganji [34] studied the magnetohydrodynamics in a nanofluid flow between two parallel plate sheets. In their analysis, they took into account both viscous dissipation and Joule heating. In their study of the magnetic field impact on a nanofluid moving buoyantly across an expanding sheet, Dogonchi and Ganji [35] showed that as thermal radiation rose, temperature fell. They showed that temperature and velocity decrease as thermal radiation rises. Mahapatra and Bandopadhyay [36] combined the pressure-driven and electroosmotic Oldroyd-B fluid in microchannels. They focused on the velocity slip flow at high zeta potential and thin EDL.

The time-dependent MHD free-convection flow controlled by the effect of injection or suction has been extensively studied recently. When fluid particles are injected through a porous wall, the drag on the boundary surfaces and the heat transfer coefficients generally seem to be increased, however, an opposite tendency is seen when suction is applied to the porous wall. Chemical reactions employ suction to remove reactants, and injection to supply reactants, chill the surface, stop corrosion or scaling, and lessen drag [37]. The impact of suction and injection on a Couette flow with varying parameters was demonstrated by Attia [38]. Magnetohydrodynamic oscillatory flow in a planar porous channel with suction and injection was theoretically analyzed by Ahmed and Khatun [39]. Magyari and Chamkha [40] offered a complete analytical solution to the combined impact of heat generation or absorption and first-order chemical reaction on micropolar fluid. Rundora and Makinde [41] studied the effects of suction/injection on unstable reactive temperature dependent viscosity in a porous channel filled with saturated porous media. Hamid *et al.* [42] used suction and injection to demonstrate the effects of radiation. Joule heating, and viscous dissipation on an MHD Marangoni convection across a flat surface. Ghasemi *et al*. [43] most recently used the least-squares approach to study an electrohydrodynamic flow in a circular cylindrical conduit. The impact of nonuniform single and double slot suction/injection on a steady mixed convection boundary layer flow around a vertical cone was examined by Ravindran and Ganapathirao [44].

Based on the aforementioned studies, the objective of this work is to investigate the impact of suction/injection on a transient electromagnetohydrodynamic natural convection flow with an electroosmotic effect in a vertical channel.

## 2. Method

### 2.1. Mathematical formulation

In a transient electromagnetohydrodynamic natural convection flow in a micro-channel, the suction/injection impact of viscous incompressible fluids is taken into account. Figure 1 depicts the physical layout and the coordinate system of the issue. Let us assume that the channel's length "$L$" is significantly bigger than its height "$H$" and width"$W$", that is $L > H$ and $L > W$. Therefore, it is feasible to disregard the velocity in the *z* direction. A homogeneous magnetic field $\vec{B}=\left(0,B_y,0\right)$ and two direct current electrical field $\vec{E}=\left(E_x,0,-E_z\right)$ are utilized. The velocity field is $\vec{U}=\left(u\left(y,t\right),0,0\right)$. The flow is produced by the interaction of the Lorentz force and electrical body force. The direct current electrical field and net density charge create the electrical body force $\rho_e\vec{E}$ and the product of the electric current and the magnetic field generates the Lorentz force $\vec{J}\times\vec{B}$, where $\vec{J} = \sigma(\vec{E} + \vec{U} \times \vec{B})$ is determined according to Ohm's equation, and $\sigma$ as is the electrical conductivity of the fluid.

The Boltzmann-Poisson equation is the same as in Saha and Kundu [45] in dimensionless form:

$$\frac{d^2\psi}{dY^2} - K^2\psi = 0\,. \tag{2.1}$$

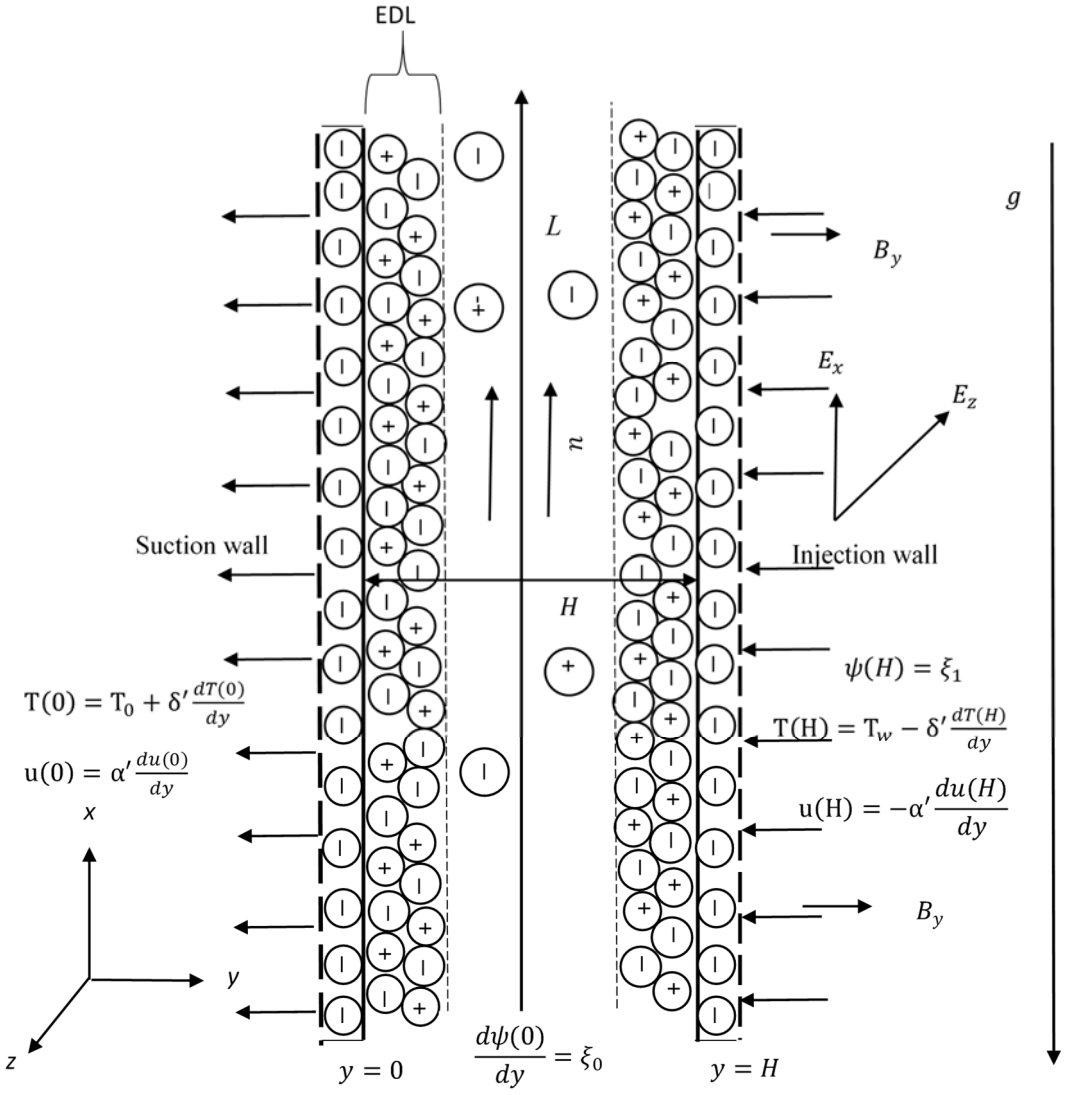


Fig.1. Visualization of the natural convection flow in a vertical parallel plate microchannel of electromagnetohydrodynamic fluid with suction/injection wall

Together with the following boundary condition for the zeta potential

$$\frac{d\psi(0)}{dY} = 0 \text{ and } \psi(1) = \xi_1 . \tag{2.2}$$

Applying the boundary conditions of (2.2) in (2.1) yields:

$$\psi = c_1 e^{KY} + c_2 e^{-KY} , \tag{2.3}$$

where

$$c_1 = \frac{\xi_1}{e^K + e^{-K}} = c_2 . \tag{2.4}$$

In the flow formation, the governing continuity equation and Navier-Stokes equation are, respectively, given in vector notations as:

$$\nabla \bullet \vec{U} = \frac{\partial u}{\partial x} + \frac{\partial v}{\partial y} + \frac{\partial w}{\partial z} = 0 . \tag{2.5}$$

$$\rho\left( \frac{\partial \vec{U}}{\partial t} + \left(\vec{U} \bullet \nabla\right)\vec{U} \right) = -\nabla P + \mu \nabla^2 \vec{U} + \vec{F}. \tag{2.6}$$

where $\mu$ fluid viscosity. The Lorentz force is the net body force that is exerted on a fluid element as a result of an applied electric field and magnetic field. The electromagnetic body force can be defined as:

$$\vec{F} = \rho_e \vec{E} + \vec{J} \times \vec{B} . \tag{2.7}$$

The electromagnetic hydrodynamic flow field's energy and momentum equations are expressed as:

i. Time periodic energy equation

$$\frac{\partial T}{\partial t} = \alpha \frac{\partial^2 T}{\partial y^2} + \nu_0 \frac{\partial T}{\partial y} + \frac{Q_0}{\rho_o C_p}\left[\sin\left(\omega t\right)\right]. \tag{2.8}$$

ii. Temperature dependent energy equation

$$\frac{\partial T}{\partial t} = \alpha \frac{\partial^2 T}{\partial y^2} + \nu_0 \frac{\partial T}{\partial y} + \frac{Q_0}{\rho_o C_p}\left(T - T_0\right). \tag{2.9}$$

iii. Momentum equation

$$\frac{\partial u}{\partial t} = \upsilon \frac{\partial^2 u}{\partial y^2} + \nu_0 \frac{\partial u}{\partial y} + g\beta\left(T - T_0\right) - \frac{\sigma {B_0}^2 u}{\rho_0} + \frac{\rho_{eE_x}}{\rho_0} + \frac{\sigma E_z B}{\rho_0}. \tag{2.10}$$

The below dimensional boundary condition is used to solve energy equations and the momentum equation:

$$t \le 0, \quad u = 0, \quad T = T_0 \quad 0 \le y \le H , \tag{2.11}$$

$$t > 0 \begin{cases} u\left(y\right) = \alpha' \dfrac{du}{dy} , \quad T\left(y\right) = T_1 + \delta' \dfrac{dT}{dy} & \text{at} \quad y = 0, \\ u\left(y\right) = -\alpha' \dfrac{du}{dy} , \quad T\left(y\right) = T_w - \delta' \dfrac{dT}{dy} & \text{at} \quad y = H. \end{cases} \tag{2.12}$$

Utilizing the dimensionless parameters in (2.13) to transform Eqs (2.8-2.12) to dimensionless equations.

$$U = \frac{uH}{\upsilon}, \quad \theta = \frac{T - T_0}{T_\omega - T_0}, \quad Y = \frac{y}{H}, \quad \zeta = \frac{t\upsilon}{H^2}, \quad Pr = \frac{\upsilon}{\alpha}, \quad \delta = \frac{\omega H^2}{\upsilon}, \quad \alpha = \frac{\alpha'}{H},$$

$$\bar{E}_x = \frac{E_x \varepsilon \varepsilon_0 \xi_1}{\rho_0 \nu^2}, \qquad \delta^* = \frac{\delta'}{H}, \qquad \xi_t = \frac{T_1 - T_0}{T_w - T_0}, \qquad H_a = BH\sqrt{\frac{\sigma}{\rho_0 \upsilon}},$$

$$Gr = \frac{g\beta(T - T_0)H^3}{\nu^2}, \qquad S_z = \frac{H^2 E_z \sqrt{\sigma}}{\upsilon\sqrt{\upsilon\rho_0}}, \qquad a = \frac{Q_0 H^2}{k(T_w - T_0)}, \tag{2.13}$$

$$b = \frac{Q_0 H^2}{k}, \qquad S_0 = \frac{v_0 \upsilon}{H}.$$

Applying Eq.(2.13) to the dimensionless energy and momentum equations below yields:
Time periodic energy equation;

$$\frac{\partial \theta}{\partial \zeta} = \frac{1}{Pr}\frac{\partial^2 \theta}{\partial Y^2} + S_0 \frac{\partial \theta}{\partial y} + \frac{1}{Pr}\left[a \sin(\delta\zeta)\right]. \tag{2.14}$$

Temperature dependent energy equation

$$\frac{\partial \theta}{\partial \zeta} = \frac{1}{Pr}\frac{\partial^2 \theta}{\partial Y^2} + S_0 \frac{\partial \theta}{\partial y} + \frac{1}{Pr}\left[b(T - T_0)\right]. \tag{2.15}$$

Momentum equation

$$\frac{\partial U}{\partial \zeta} = \frac{\partial^2 U}{\partial y^2} + S_0 \frac{\partial U}{\partial y} + Gr\theta - Ha^2 U + S_z H_a - \bar{E}xK^2\psi. \tag{2.16}$$

$$t \le 0, \quad \theta = 0, \quad U = 0 \forall Y. \tag{2.17}$$

$$t > 0 \begin{cases} U(Y) = \alpha\dfrac{dU}{dY}, \qquad \theta(Y) = \xi_t + \delta^*\dfrac{d\theta}{dY} & \text{at} \quad Y = 0, \\ U(Y) = -\alpha\dfrac{dU}{dY}, \qquad \theta(Y) = 1 - \delta^*\dfrac{d\theta}{dY} & \text{at} \quad Y = 1. \end{cases} \tag{2.18}$$

### 2.2. Analytical solution

We used the Laplace transformation method to convert equations (2.14) to (2.18) from PDEs to ODEs in order to solve the two dimensionless energy equations and momentum equation together with their dimensionless boundary conditions:
Dimensionless time periodic energy equation;

$$\frac{d^2\hat{\theta}}{dY^2} + S_0 Pr\frac{d\hat{\theta}}{dY} - SPr\hat{\theta} = -\frac{a\delta}{S^2 + \delta^2}. \tag{2.19}$$

Dimensionless temperature-dependent energy equation;

$$\frac{d^2\hat{\theta}}{dY^2} + S_0 Pr \frac{d\hat{\theta}}{dY} - SPr\hat{\theta} + b\hat{\theta} = 0. \tag{2.20}$$

Dimensionless momentum equation;

$$\frac{d^2\hat{U}}{dY^2} + S_0 \frac{d\hat{U}}{dY} - \left[ Ha^2 + S \right]\hat{U} = \frac{\bar{E}_x K^2}{S}\left( c_1 e^{KY} + c_2 e^{-KY} \right) - \frac{S_z Ha}{S} - Gr\hat{\theta}. \tag{2.21}$$

where $S$ is a Laplace transform parameter, while $\hat{\theta}$ and $\hat{U}$ are the temperature and velocity, respectively, in the Laplace domain, subject to:

$$t > 0 \begin{cases} \hat{\theta} = \dfrac{\xi_t}{s} + \delta^* \dfrac{d\hat{\theta}}{\partial Y}, \ \hat{U} = \delta^* \dfrac{\partial \hat{U}}{\partial Y} & \text{at} \quad Y = 0, \\ \hat{\theta} = \dfrac{1}{S} - \delta^* \dfrac{d\hat{\theta}}{\partial Y}, \ \hat{U} = -\delta^* \dfrac{\partial \hat{U}}{\partial Y} & \text{at} \quad Y = 1. \end{cases} \tag{2.22}$$

The method of undetermined coefficient was applied to solve Eqs (2.19) to (2.21) as shown below.

### 2.2.1. Time periodic case

Solutions of temperature and velocity

$$\hat{\theta} = c'_3 e^{g_1 Y} + c'_4 e^{g_2 Y} + a_2. \tag{2.23}$$

$$\hat{U} = c'_5 e^{j_1 Y} + c'_6 e^{j_2 Y} + j_3 e^{g_1 Y} + j_4 e^{g_2 Y} + j_5 e^{kY} + j_6 e^{-kY} + d_4 + d_7. \tag{2.24}$$

$$c'_3 = \frac{a_5 g_6 - a_8 g_4}{g_3 g_6 - g_5 g_4}, \ c'_4 = \frac{a_5 g_5 - a_8 g_3}{g_4 g_5 - g_6 g_3}, \ c'_5 = \frac{m_3 m_5 - m_6 m_2}{m_1 m_5 - m_4 m_2}, \ c'_6 = \frac{m_3 m_4 - m_6 m_1}{m_2 m_4 - m_5 m_1}. \tag{2.25}$$

The skin friction at $Y = 0$ and $Y = 1$ of the micro-channel is given by:

$$\hat{\tau}_0 = \frac{d\hat{U}(0)}{dY} = j_1 c'_5 + j_2 c'_6 + g_1 j_3 + g_2 j_4 + j_5 k - j_6 k. \tag{2.26}$$

$$\hat{\tau}_1 = -\frac{d\hat{U}(1)}{dY} = -\left( j_1 c'_5 e^{j_1} + j_2 c'_6 e^{j_2} + g_1 j_3 e^{g_1} + g_2 j_4 e^{g_2} + d_5 k e^{k} - d_6 k e^{-k} \right). \tag{2.27}$$

The mass flow rate $(Q)$ is given as:

$$\hat{Q} = \int_0^1 \hat{U}(Y)\,dY = \frac{c'_5\left(e^{j_1}-1\right)}{j_1} + \frac{c'_5\left(e^{j_2}-1\right)}{j_2} + \frac{j_3\left(e^{g_1}-1\right)}{g_1} - \\ + \frac{j_3\left(e^{g_2}-1\right)}{g_2} + \frac{j_5\left(e^{k}-1\right)}{k} - \frac{j_6\left(e^{-k}-1\right)}{k} + d_4 + d_7. \tag{2.28}$$

### 2.2.2. Temperature dependent case

Solutions of temperature and velocity:

$$\hat{\theta}_* = c'_{*3}\,e^{h_1 Y} + c'_{*4}\,e^{h_2 Y}. \tag{2.29}$$

$$\hat{U}_* = c'_{*5}\,e^{j_1 Y} + c'_{*6}\,e^{j_2 Y} + n_1 e^{h_1 Y} + n_2 e^{h_2 Y} + j_5 e^{kY} + j_6 e^{-kY} + d_7. \tag{2.30}$$

$$c'_{*3} = \frac{b_4 h_6 - b_7 h_4}{h_3 h_6 - h_5 h_4}, \quad c'_{*4} = \frac{b_4 h_5 - b_7 h_3}{h_4 h_5 - h_6 h_3}, \quad c'_{*5} = \frac{n_5 n_7 - n_8 n_4}{n_3 n_7 - n_6 n_4}, \quad c'_{*6} = \frac{n_5 n_6 - n_8 n_3}{n_4 n_6 - n_7 n_3}. \tag{2.31}$$

The skin friction at $Y = 0$ and $Y = 1$ of the micro-channel is given by:

$$\hat{\tau}'_{*0} = \frac{d\hat{U}_*(0)}{dY} = j_1 c'_{*5} + j_2 c'_{*6} + h_1 n_1 + h_2 n_2 + j_5 k - j_6 k. \tag{2.32}$$

$$\hat{\tau}'_{*1} = -\frac{d\hat{U}_*(1)}{dY} = -\left(j_1 c'_{*5} e^{j_1} + j_2 c'_{*6} e^{j_2} + h_1 n_1 e^{h_1} + h_2 n_2 e^{h_2} + d_5 k e^{k} - d_6 k e^{-k}\right). \tag{2.33}$$

The mass flow rate $(Q)$ is given as:

$$\widehat{Q}'_* = \int_0^1 \hat{U}(Y)\,dY = \frac{c'_{*5}\left(e^{d_1}-1\right)}{d_1} - \frac{c'_{*5}\left(e^{-d_1}-1\right)}{d_1} + \frac{p_1\left(e^{b_1}-1\right)}{b_1} - \\ + \frac{p_2\left(e^{-a_1}-1\right)}{b_2} + \frac{d_5\left(e^{k}-1\right)}{k} - \frac{d_6\left(e^{-k}-1\right)}{k} + d_7. \tag{3.34}$$

### 2.3. Riemann-sum approximation (RSA)

To achieve the goal of the article, it is required to convert the analytical solutions of Eqs (2.23)-(2.34), which are in the Laplace domain to the time domain. A numerical approach based on the Riemann-sum approximation (RSA) as used in Jha and Apere [46], Jha and Oni [47], Khadrawi and Al-Nimr [48], and Tzou [49] is employed. The numerical the Laplace inversion approach, according to Jha and Oni [47] has shown to be a dependable and practical instrument for Laplace inversion. This technique inverts the temperature distribution, velocity profile, skin friction, and mass flux, which are all in the Laplace domain, to the time domain.

### 2.3.1. Time periodic (TP) case

$$\theta(Y,\zeta) = \frac{e^{\varepsilon\zeta}}{\zeta}\left[\frac{1}{2}\hat{\theta}(y,\varepsilon)_{TP} + Re\sum_{n=1}^{E}\hat{\theta}\left(Y,\varepsilon+\frac{in\pi}{\zeta}\right).(-1)^n\right], \quad 0 \le Y \le 1. \tag{2.35}$$

$$U(Y,\zeta)=\frac{e^{\varepsilon\zeta}}{\zeta}\left[\frac{1}{2}\hat{U}(y,\varepsilon)_{TP}+Re\sum_{n=1}^{E}\hat{U}\left(Y,\varepsilon+\frac{in\pi}{\zeta}\right).(-1)^{n}\right],\quad 0\le Y\le 1. \tag{2.36}$$

Skin friction

$$\tau_0=\frac{e^{\varepsilon\zeta}}{\zeta}\left[\frac{1}{2}\hat{\tau}_0(0,\varepsilon)+Re\sum_{n=1}^{E}\hat{\tau}_0\left(0,\varepsilon+\frac{in\pi}{\zeta}\right)(-1)^{n}\right],\quad Y=0. \tag{2.37}$$

$$\tau_1=\frac{e^{\varepsilon\zeta}}{\zeta}\left[\frac{1}{2}\hat{\tau}_1(0,\varepsilon)+Re\sum_{n=1}^{E}\hat{\tau}_1\left(1,\varepsilon+\frac{in\pi}{\zeta}\right)(-1)^{n}\right],\quad Y=1. \tag{2.38}$$

Mass flow rate

$$Q(\zeta)=\frac{e^{\varepsilon\zeta}}{\zeta}\left[\frac{1}{2}\hat{Q}(\varepsilon)+Re\sum_{n=1}^{E}\hat{Q}\left(\varepsilon+\frac{in\pi}{\zeta}\right)(-1)^{n}\right],\quad 0\le Y\le 1. \tag{2.39}$$

### 2.3.2. Temperature dependent (TD) case

$$\theta_*(Y,\zeta)=\frac{e^{\varepsilon\zeta}}{\zeta}\left[\frac{1}{2}\hat{\theta}_*(Y,\varepsilon)_{TD}+Re\sum_{n=1}^{E}\hat{\theta}_*\left(Y,\varepsilon+\frac{in\pi}{\zeta}\right).(-1)^{n}\right],\quad 0\le Y\le 1. \tag{2.40}$$

$$U_*(Y,\zeta)=\frac{e^{\varepsilon\zeta}}{\zeta}\left[\frac{1}{2}\hat{U}_*(y,\varepsilon)_{TD}+Re\sum_{n=1}^{E}\hat{U}_*\left(Y,\varepsilon+\frac{in\pi}{\zeta}\right).(-1)^{n}\right],\quad 0\le Y\le 1. \tag{2.41}$$

Skin friction temperature dependent case

$$\tau'_{*0}=\frac{e^{\varepsilon\zeta}}{\zeta}\left[\frac{1}{2}\hat{\tau}'_{*0}(0,\varepsilon)+Re\sum_{n=1}^{E}\hat{\tau}'_{*0}\left(0,\varepsilon+\frac{in\pi}{\zeta}\right).(-1)^{n}\right],\quad Y=0. \tag{2.42}$$

$$\tau'_{*1}=\frac{e^{\varepsilon\zeta}}{\zeta}\left[\frac{1}{2}\hat{\tau}'_{*1}(0,\varepsilon)+Re\sum_{n=1}^{E}\hat{\tau}'_{*1}\left(1,\varepsilon+\frac{in\pi}{\zeta}\right)(-1)^{n}\right],\quad Y=1. \tag{2.43}$$

Mass flow rate

$$Q'_*(\zeta)=\frac{e^{\varepsilon\zeta}}{\zeta}\left[\frac{1}{2}\hat{Q}'_*(0,\varepsilon)+Re\sum_{n=1}^{E}\hat{Q}'_*\left(Y,\varepsilon+\frac{in\pi}{\zeta}\right)(-1)^{n}\right]. \tag{2.44}$$

## 3. Results and discussions

With the help of the MATLAB program version R2014a, the findings and explanation of the dimensionless and semi-analytical solutions obtained in section 2 are presented graphically.

### 3.1. Results and discussion of the problem

The effect of dimensionless time $(\zeta)$, Prandtl number $(Pr)$, Hartmann number $(Ha)$ Grasshof number $(Gr)$ electric field strength $(S_z)$ and $(\bar{E}_x)$ on temperature and velocity profile for suction and injection scenario on time-periodic and temperature-dependent cases are graphically presented in figures. Furthermore, parameters affecting suction and injection in skin friction $(\tau_0, \tau_1)$, and mass flow rate $(Q)$ are presented graphically also. During the computation, the numerical value for $\zeta$ and $Pr$ are as follows; unless otherwise stated: time $0.2 \le \zeta \le 5.0$ and Prandtl numbers $(Pr)$ are $Pr = 0.71$ (air) and $Pr = 7.0$ (water). The reference values for the time parameter $(\zeta)$, $Pr$, $Ha$, $Gr$, $(S_z)$ and $(\bar{E}_x)$ are *5.0*, *0.71*, *2.0*, *1.0*, *2* and *-2*, respectively. The effect of the Debye-Huckel parameter $(\kappa)$ on the electric potential in the microchannel for a symmetric zeta-potential condition is depicted in Fig.2. It was found that when K rises in the microchannel, the electric potential falls. It was discovered that the wall $Y = 1$ of the microchannel had the highest electric potential. This is consistent with the zeta-potential requirement prescribed at the wall $Y = 1$.

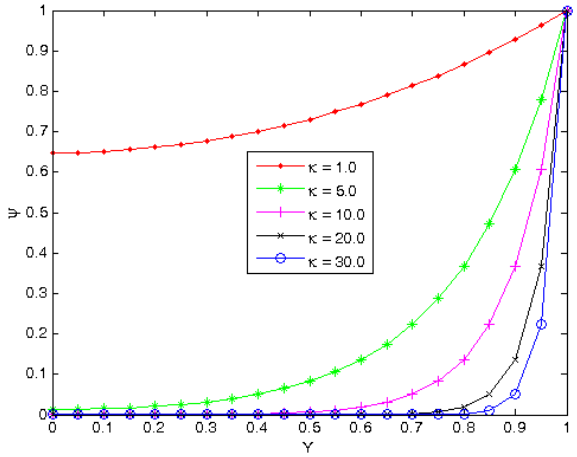


Fig.2. Electric potential for different values of $\kappa$.

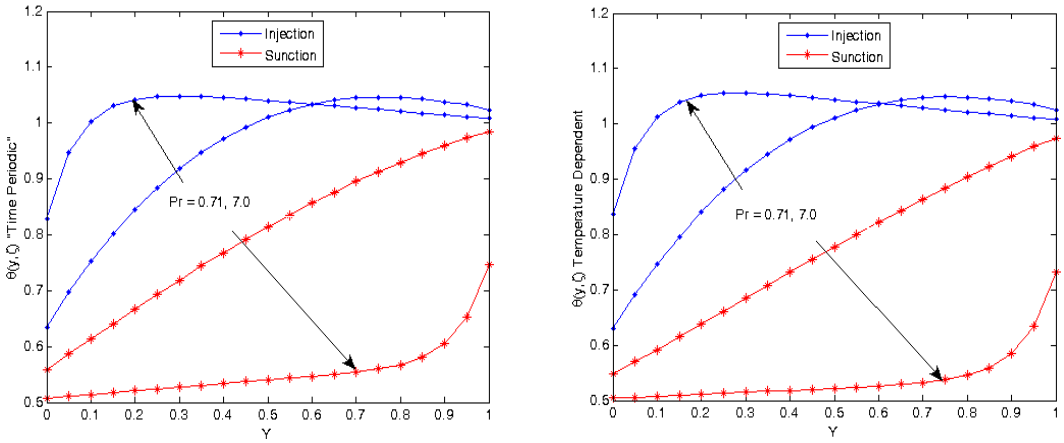


(A) (B)

Fig.3. Temperature distribution for $Pr = 0.71$ and $7.0$.

The effect of $Pr$ on the temperature distribution is shown in Fig.3. Fig. 3A takes into account the time-periodic condition, whereas Fig.3B depicts the temperature-dependent situation. Both figures

demonstrated that the temperature was larger when $Pr = 7.0$ than when $Pr = 0.71$ in injection scenario while it was larger when $Pr = 0.71$ than when $Pr = 7.0$ in suction situation. The cause of this behavior is thought to be the injection of fluid particles through the permeable wall, which displace the cold fluid and raise the temperature in the microchannel. Clearly, the two figures showed that $Pr$ has a similar effect in time-periodic and temperature dependent cases.

The influence of time $(\zeta)$ on the temperature distribution is presented in Fig.4. The time-periodic situation is illustrated in Fig.4A, where the temperature is continuously fluctuating as $\zeta$ increases. This is as a result of its time-periodic character in the system. Fig. 4B is applicable for the temperature-dependent scenario; it demonstrates how the temperature rises with an increase in $\zeta$ and reaches a steady state as $\zeta \to \infty$. Additionally, injection temperatures are greater than suction temperatures, which is consistent with assumption that the injection of fluid particles through the permeable wall, displaces the cold fluid and raises the temperature in the microchannel.

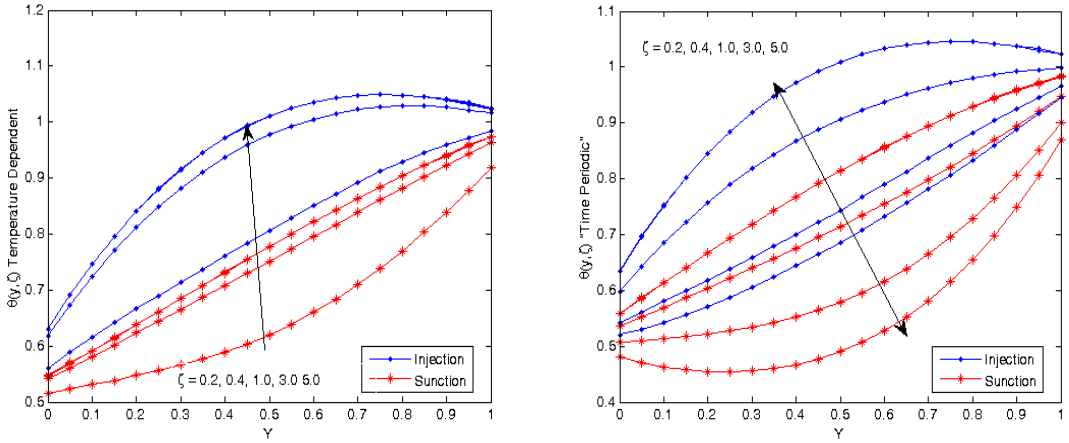


(A) (B)

Fig.4. Temperature distribution for different values of time $(\zeta)$.

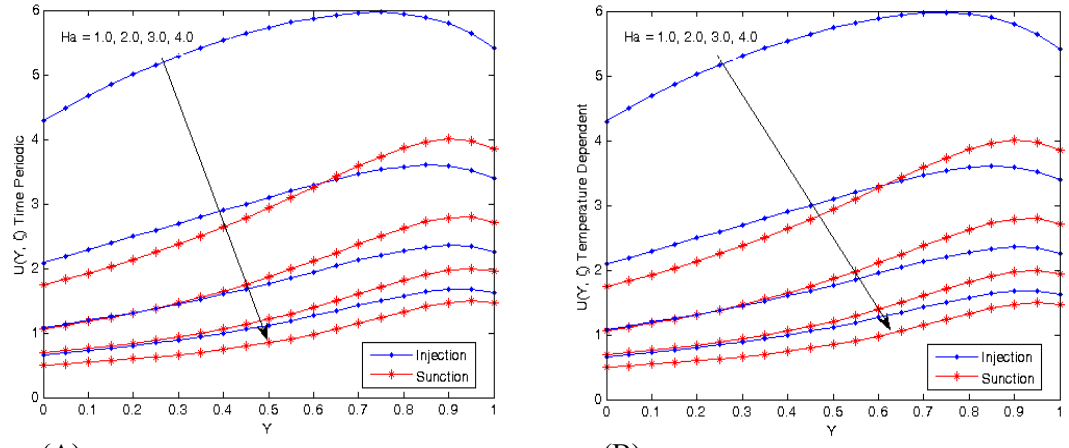


(A) (B)

Fig.5. Velocity profile for different values of $Ha$.

The Hartmann number $Ha$'s influence on the velocity profile is seen in Fig.5. Fig. 5A shows how $Ha$ affected the time-periodic instance, whereas Fig.5B shows how $Ha$ contributed to the temperature-dependent instance. It is clear from both figures that a rise in $Ha$ causes a fall in fluid velocity while a fall in $Ha$ causes a rise in fluid velocity. It is true that $Ha$ reduces fluid velocity because the Lorentz force opposes fluid velocity.

The consequence of the Grashof number $(Gr)$ on fluid velocity is shown in Fig.6. The time periodic scenario is illustrated in Fig.6A, while the temperature-dependent situation was made clear in Fig.6B. As seen in the two figures, a rise in $Gr$ causes the fluid velocity to increase in both situations, whereas a reduction in $Gr$ causes the velocity to decrease. This is due to weakening of bonds between fluids because of the rise in temperature of the walls caused by an increase in $Gr$, which also made it possible for velocity to be much higher in the injection wall than in the suction wall.

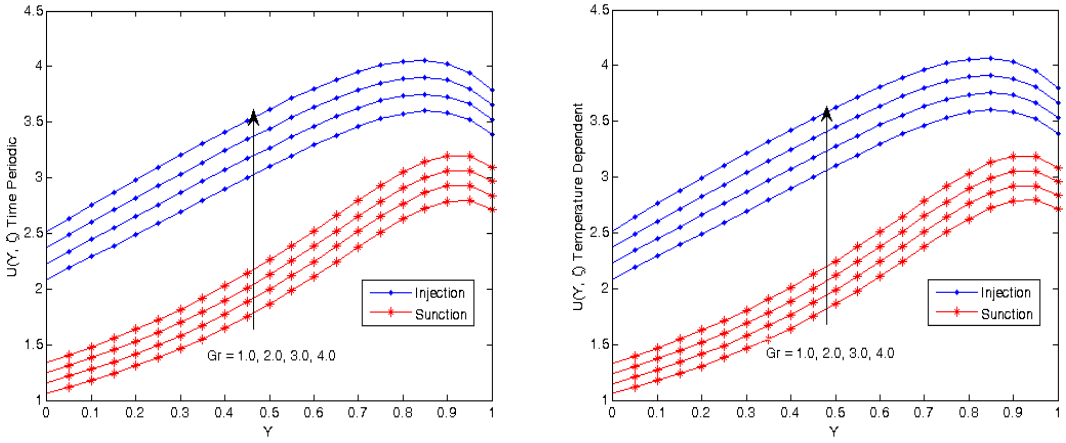


(A) (B)

Fig.6. Velocity profile for different values of $(Gr)$.

The impact of electric field strength $(Sz)$ in the *z*-direction on the velocity profile is shown in Fig.7. Figure 7A illustrates the effects of $Sz$ in the time-periodic scenario, while Fig.7B shows $Sz's$ behavior in the temperature-dependent situation. The two graphs clearly demonstrate that when $Sz$ grows, velocity increases. This is correct because a greater velocity profile caused by an increase in $Sz$ might result in stronger auxiliary forces in the electric and magnetic fields.

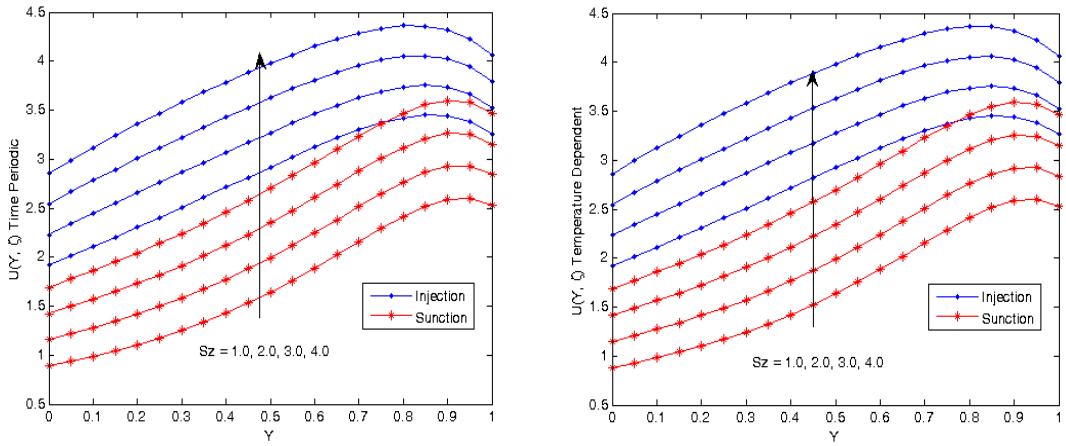


(A) (B)

Fig.7. Velocity profile for different values of $(Sz)$.

Figures 8A and 8B show, for temperature-dependent and time-periodic velocity profiles, respectively, how the electric field $(\bar{E}x)$ affects the velocity profile. In these figures, it can be seen that a drop in $\bar{E}x$ results in an increase in the velocity profile whereas an increase in $\bar{E}x$ results in a decrease in the velocity profile. This is

due to the fact that as $\overline{Ex}$ grows, stronger auxiliary forces in the electric and magnetic field might appear, which causes a drop in velocity profile.

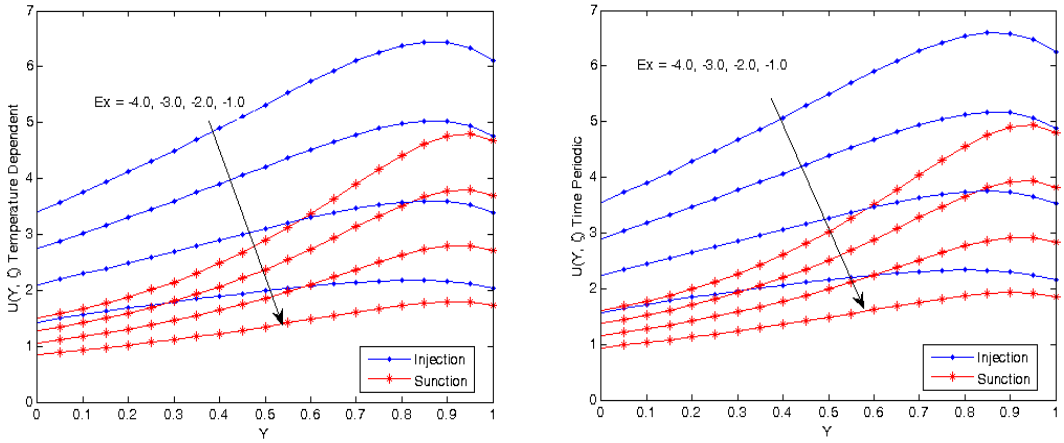


(A) (B)

Fig.8. Velocity profile for different values of $\left(\overline{Ex}\right)$.

Figures 9A and 9B show the impact of time $(\zeta)$ for time-periodic and temperature-dependent situations, respectively in the flow formation. Fig. 9A makes it evident that the velocity profile keeps increasing with $\zeta$, and then alternates when $\zeta \to \infty$. This is caused by the time periodicity of velocity. On the other hand, Fig.9B shows that the velocity increases as $\zeta$ rises and attains a steady state $\zeta \to \infty$.

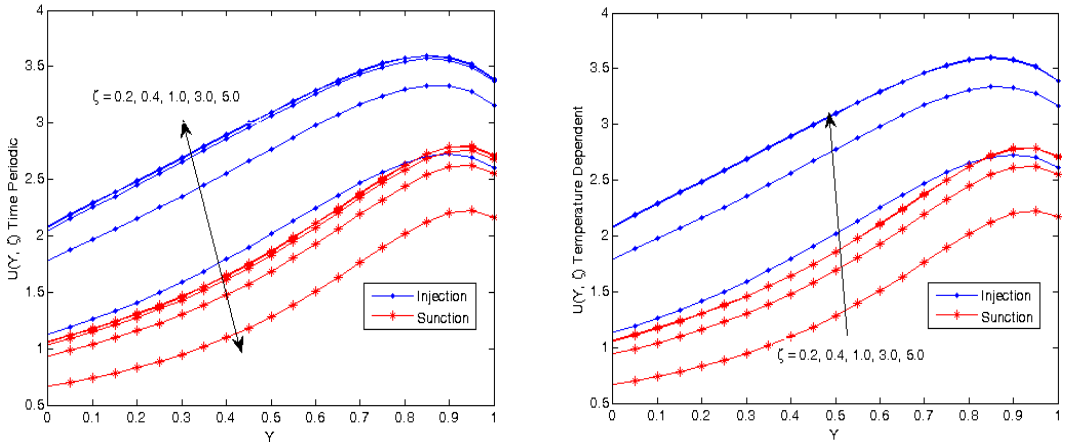


(A) (B)

Fig.9. Velocity profile for different values of time $(\zeta)$.

The impact of the symmetric wall zeta-potential on the velocity profile for various values of $K$ is shown in Fig.10, while Fig.10B shows the temperature-dependent situation, Fig.10A shows the time-periodic scenario. The aforementioned figures show that, for smaller values of $K$, the formation of flow is independent of the magnitude of the wall symmetric zeta potential. However, the effect of $K$ on flow formation is to increase the microchannel's velocity profile. This might be described by the presence of random EDL forces on the microchannel's walls, which accelerate fluid velocity.

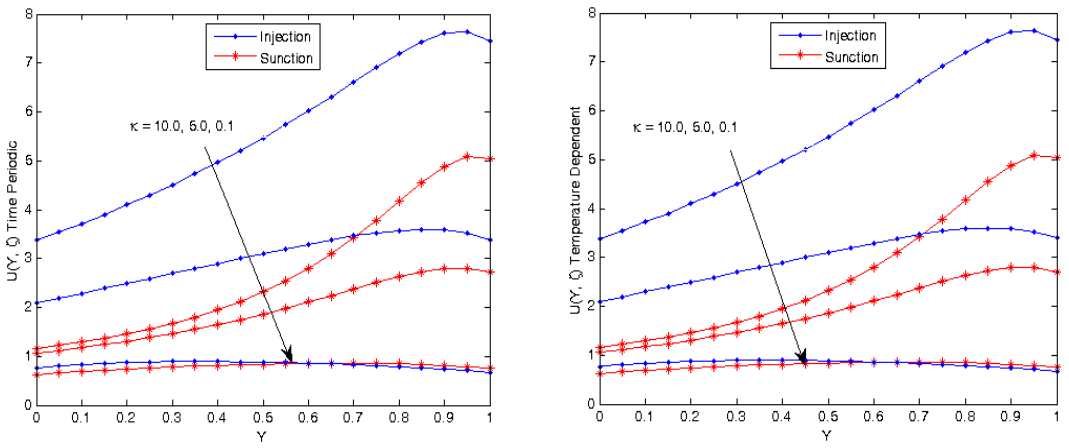


(A) (B)

Fig.10. Velocity profile for different values of $(\mathrm{K})$.

Figures 11A and 11B demonstrate the joint effect of time $(\zeta)$ and $\mathrm{K}$ on the skin-friction at $Y=0$ in time-periodic and temperature-dependent cases, respectively. These figures show that the skin friction rises as $\zeta$ and $\mathrm{K}$ grow. It is essential to see that the skin-friction alternates when $\zeta \to \infty$ in the time-periodic case and attains a steady state in the temperature-dependent case. It is noteworthy to observe, however, that for high values of $\mathrm{K}$ in the suction wall, the skin friction is only weakly reliant on $\mathrm{K}$. This is because the electrokinetic influence on the skin friction is eliminated as $\mathrm{K} \to \infty$ and the EDL length eventually goes to zero.

Figures 12A and 12B exhibit the joint effect of time $(\zeta)$ and $\mathrm{K}$ on the skin-friction at $Y=1$ in time-periodic and temperature-dependent cases, respectively. These figures show that the skin friction rises as $\zeta$ and $\mathrm{K}$ grow. It is crucial to see that the skin-friction alternates when $\zeta \to \infty$ in the time-periodic case and attains a steady state in the temperature-dependent case.

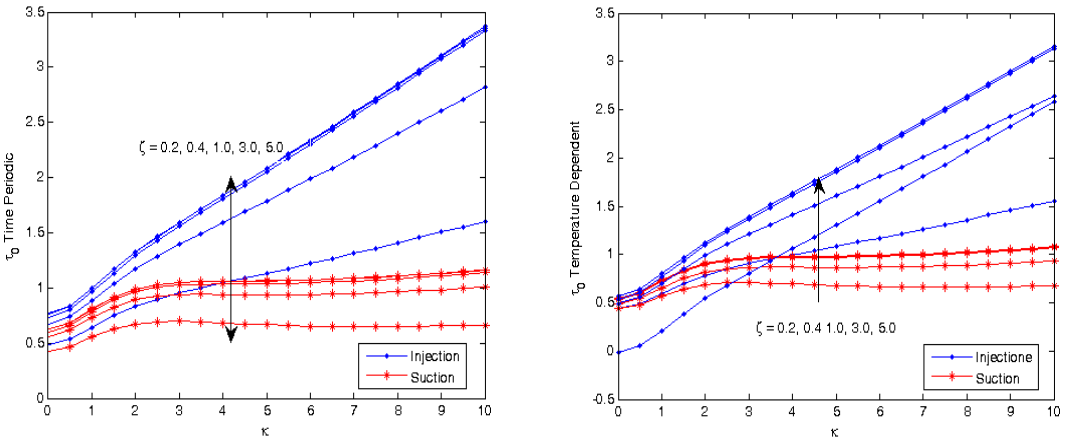


(A) (B)

Fig.11. Skin-friction for combined effect of $\mathrm{K}$ and $\zeta$ at $Y=0$.

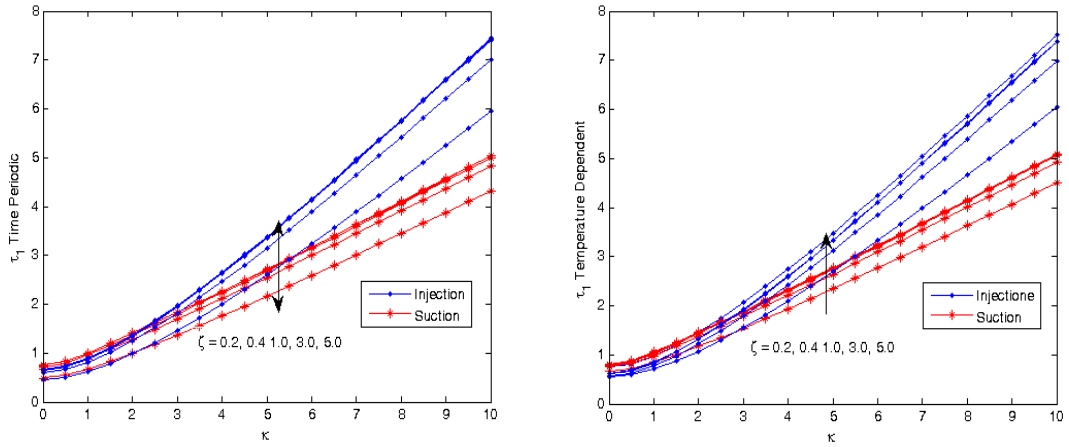


(A) (B)

Fig.12. Skin-friction for the combined effect of $K$ and $\zeta$ at $Y = 1$.

The combined impact of $K$ and $\zeta$ on the mass flow rate is seen in Fig.13. The time-periodic instance in the mass flow rate is illustrated in Fig13A for different values of $K$ and $\zeta$. It is clear from the figure that a rise in $K$ increases the mass flow rate likewise the flow rate increases as $\zeta$ increases, then oscillates as $\zeta \to \infty$. The fact that the mass flow rate increases with an increase in $K$ is due to the role of $K$ in enhancing the velocity profile. The temperature-dependent case in the mass flow rate is shown in Fig.13B for different values of $K$ and $\zeta$. It was observed from the figure that an increase in $K$ boosts the mass flow rate, also the mass flow rate increases when $\zeta$ increases and reaches a steady state as $\zeta \to \infty$.

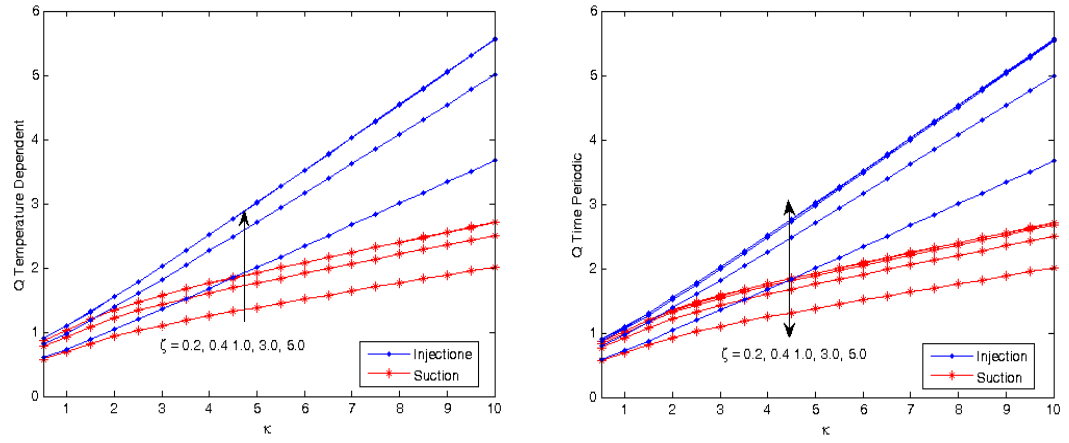


(A) (B)

Fig.13. Mass flow rate for the combined effect of $K$ and $\zeta$.

## 4. Conclusion

The unsteady electromagnetohydrodynamic natural convection flow with electroosmotic effect through a vertical plate with slip coefficient at the walls is analyzed. The second order PDE governing the energy and momentum equations are transformed to ordinary differential equation (ODE) using the Laplace transform method. A semi-analytical solution is obtained by the Riemann Sum Approximation (RSM). The changes of the dimensionless velocity profiles for various parameters are visually presented and thoroughly described. From the results of the theoretical study discussed herein, the following are key conclusions that may be succinctly made.

1. The fluid velocity increases as the Hartmann number ($Ha$) and electric field parameter $\left(\bar{E}x\right)$ drop, and decreases when they rise.
2. A rise in $Gr$ and $S_z$ as well as an increase in $\zeta$ contribute to an increase in velocity.
3. The variation of $\mathrm{K}$ and $\zeta$ in the skin-friction is shown graphically and interpreted,
4. The mass flow rate is also shown and presented in terms of $\mathrm{K}$ and $\zeta$, graphs indicate how changes in $\mathrm{K}$ and $\zeta$ directly affect the flow rate.

The findings of Oni and Jha [16], Wang *et al.* [19] and Kundu and Saha [45] are all in agreement with this study. However, it is important to note that the current study modifies Wang [19] and Kundu and Saha [45] by taking into account a transient natural convection flow in EMHD.

## Nomenclature

$a$ – heat source/sink parameter (time-periodic)
$b$ – heat source/sink parameter (temperature-dependent)
$B_0$ – constant applied magnetic field
$E_x$ – electric field in $x$ direction
$\bar{E}_x$ – electric field (dimensionless)
$E_z$ – electric field in $z$ direction
$Gr$ – Grashof number
$g$ – gravity acceleration
$H$ – distance
$Ha$ – Hartmann number (dimensionless magnetic field parameter)
$Pr$ – Prandtl number
$Q$ – mass flow rate (dimensionless)
$Q_0$ – dimensional heat source
$S$ – Laplace parameter
$S_0$ – suction/injection parameter
$S_z$ – electric strength in $z$ direction (dimensionless)
$T$ – dimentional temperature of the fluid
$T_0$ – initial temperature (dimentional)
$T_w$ – wall temperature (dimentional)
$t$ – time of flow (dimentional)
$u$ – dimensional velocity of the fluid
$U$ – dimensionless velocity

Greek symbols

$\alpha'$ – thermal diffusivity
$\alpha$ – dimensionless thermal diffusivity
$\beta$ – coefficient of thermal expansion
$\delta$ – constant rotational velocity
$\delta'$ – dimensional temperature jump-length
$\delta^*$ – dimensionless temperature jump-length
$\varepsilon$ – permittivity of space
$\varepsilon_0$ – permittivity of medium
$\zeta$ – dimensionless time

$\xi_0, \xi_1$ – zeta-potential
$\xi_t$ – Buoyancy force parameter (dimensionless)
$\theta$ – temperature of the fluid (dimensionless)
K – Debye–Hückel constant
$\rho_e$ – charge density
$\rho_0$ – fluid density
$\sigma$ – electrical conductivity of the fluid
$\tau$ – skin friction
$\psi$ – electric potential
$\upsilon$ – kinematic viscosity
$\omega$ – frequency of time-periodic heating

## APPENDIX

$$a_1 = \sqrt{(SPr - b)}, \quad a_2 = \delta\alpha, \quad a_3 = \left(S^2 + \delta^2\right)(SPr - b), \quad a_4 = \frac{a_2}{a_3}, \quad b_1 = (1 - \lambda Kna_1),$$

$$b_2 = (1 + \lambda Kna_1), \quad b_3 = e^{a_1} + \lambda Kna_1 e^{a_1}, \quad b_4 = e^{-a_1} - \lambda Kna_1 e^{-a_1}, \quad b_5 = \frac{\gamma}{S} - a_4, \quad b_6 = \frac{\xi}{S} - a_4,$$

$$d_1 = \sqrt{(Ha^2 + S)}, \quad d_2 = \frac{\bar{E}zK^2 C_1}{S[K^2 - \left(\left(Ha^2 + S\right)\right]}, \quad d_3 = \frac{S_z Ha}{S\left(Ha^2 + S\right)}, \quad d_4 = \frac{-GrC_3}{[a_1^2 - \left(\left(Ha^2 + S\right)\right]},$$

$$d_5 = \frac{-GrC_4}{[a_1^2 - \left(\left(Ha^2 + S\right)\right]}, \quad d_6 = \frac{Gra_4}{\left(Ha^2 + S\right)}, \quad d_7 = d_2 \cosh(k) + d_3 + d_4 e^{a_1} + d_5 e^{-a_1} + d_6$$

$$f_1 = \delta_2 d_1, \quad f_2 = -\delta_2 d_1, \quad f_3 = a_1 \delta_2 d_4, \quad f_4 = -a_1 \delta_2 d_5, \quad g_1 = \delta_4 d_1 e^{d_1}, \quad g_2 = -\delta_4 d_1 e^{-d_1},$$

$$g_3 = \delta_4 d_2 K sinh(K), \quad g_4 = \delta_4 d_4 a_1 e^{a_1}, \quad g_5 = -\delta_4 d_5 a_1 e^{-a_1}, \quad g_6 = g_3 + g_4 + g_5,$$

$$h_1 = 1 - f_1, \quad h_2 = 1 - f_2, \quad h_3 = \frac{\delta_1}{S} + f_3 + f_4 - (d_2 + d_3 + d_4 + d_5 + d_6),$$

$$j_1 = e^{d_1} + g_1, \quad j_2 = e^{-d_1} + g_2, \quad j_3 = \frac{\delta_3}{S} - g - d_7,$$

$$g_1 = \frac{-s_0 Pr + \sqrt{(s_0 \mathrm{Pr})^2 + 4Spr}}{2}, \quad g_2 = \frac{-s_0 Pr - \sqrt{(s_0 \mathrm{Pr})^2 + 4Spr}}{2}, \quad a_2 = \frac{Aa\delta}{SPr\left(S^2 + \delta^2\right)},$$

$$g_3 = \left(1 - \delta^* g_1\right), \quad g_4 = \left(1 - \delta^* g_2\right), \quad a_5 = \frac{\xi_t}{s} - a_2,$$

$$g_5 = \left(e^{g_1} + \alpha g_1 e^{g_1}\right), \qquad g_6 = \left(e^{g_2} + \alpha g_2 e^{g_2}\right), \qquad a_8 = \frac{1}{s} - a_2,$$

$$h_1 = \frac{-s_0 Pr + \sqrt{(s_0 \mathrm{Pr})^2 + 4(Spr - Ab)}}{2}, \qquad h_2 = \frac{-s_0 Pr - \sqrt{(s_0 \mathrm{Pr})^2 + 4(Spr - Ab)}}{2}. \qquad h_3 = \left(1 - \delta^* h_1\right),$$

$$h_4 = \left(1 - \delta^* h_2\right), \; h_5 = \left(e^{h_1} + \alpha h_1 e^{h_1}\right), \qquad h_6 = \left(e^{h_2} + \alpha h_2 e^{h_2}\right), \qquad b_4 = \frac{\xi_t}{s}, \qquad b_7 = \frac{1}{s},$$

$$j_1 = \frac{-s_0 + \sqrt{(s_0)^2 + 4\left(Ha^2 + s\right)}}{2}, \qquad j_2 = \frac{-s_0 - \sqrt{(s_0)^2 + 4\left(Ha^2 + s\right)}}{2}, \qquad j_3 = \frac{-Grc'_3}{g_1{}^2 + s_0 g_1 - \left(Ha^2 + s\right)},$$

$$j_4 = \frac{-Grc'_4}{g_2{}^2 + s_0 g_2 - \left(Ha^2 + s\right)}, \qquad j_5 = \frac{\bar{E}_x k^2 c_1}{s\left[k^2 + s_0 k - \left(Ha^2 + s\right)\right]}, \qquad j_6 = \frac{\bar{E}_x k^2 c_2}{s\left[k^2 - s_0 k - \left(Ha^2 + s\right)\right]},$$

$$m_1 = \left(1 - \alpha j_1\right), \qquad m_2 = \left(1 - \alpha j_2\right), \qquad m_3 = \alpha g_1 j_3 + \alpha g_2 j_4 + \alpha j_5 k - \alpha j_6 k - \left(j_3 + j_4 + j_5 + 6_6 + d_4 + d_7\right),$$

$$m_4 = \left(e^{j_1} + \alpha j_1 e^{j_1}\right), \; m_5 = \left(e^{j_2} + \alpha j_2 e^{j_2}\right),$$

$$m_6 = -\alpha g_1 j_3 e^{g_1} - \alpha g_2 j_4 e^{g_2} - \alpha j_5 k e^{k} + \alpha j_6 k e^{-k} - \left(j_3 e^{g_1} + j_4 e^{g_2} + j_5 e^{k} + j_6 e^{-k} + d_4 + d_7\right),$$

$$d_4 = \frac{Gra_2}{\left(Ha^2 + s\right)}, \qquad d_7 = \frac{s_z Ha}{s\left[Ha^2 + s\right]},$$

$$n_1 = \frac{-Grc'_{*3}}{h_1{}^2 + s_0 h_1 - \left(Ha^2 + s\right)}, \qquad n_2 = \frac{-Grc'_{*4}}{h_2{}^2 + s_0 h_2 - \left(Ha^2 + s\right)}, \qquad n_3 = \left(1 - \alpha j_1\right), \qquad n_4 = \left(1 - \alpha j_2\right),$$

$$n_5 = \alpha n_1 h_1 + \alpha n_2 h_2 + \alpha j_5 k - \alpha j_6 k - \left(n_1 + n_2 + j_5 + 6_6 + d_7\right), \qquad n_6 = \left(e^{j_1} + \alpha j_1 e^{j_1}\right), \qquad n_7 = \left(e^{j_2} + \alpha j_2 e^{j_2}\right),$$

$$n_8 = -\alpha n_1 h_1 e^{h_1} - \alpha n_2 h_2 e^{h_2} - \alpha j_5 k e^{k} + \alpha j_6 k e^{-k} - \left(n_1 e^{h_1} + n_2 e^{h_2} + j_5 e^{k} + j_6 e^{-k} + d_7\right).$$

## References


[1] Cramer K.R. and Pai S.I. (1973): *Magnetofluid Dynamics for Engineers and Applied Physicists*.– McGraw-Hill Book Company, vol.5, No.17.

[2] Jang J. and Lee S.S. (2000): *Theoretical and experimental study of MHD (magnetohydrodynamics) micropump*.– Elsavier, vol.80, No.1, pp.84-89.

[3] Davidson P.A (2001): *An Introduction to Magnetohydrodynamics*.– Cambridge U. Press., vol.70, No.7, pp.431.

[4] Li D. (2008): *Encyclopedia of Microfluidics and Nanofluidics*.– Springer.

[5] Mitra S., Maity S., Sutradhar S. and Bandyopadhyay D. (2020): *Electroosmosis with augmented mixing in rigid to flexible microchannels with surface pattern*.– Ind. Eng. Chem., vol.59, No.9, pp.3717-3792.

[6] Lemoff A.V. and Lee A.P. (2000): *An AC magnetohydrodynamic micropump*.– Sens. Actuator B-Chem., vol.63, No.3, pp.178-185.

[7] Chakraborty S. and Paul D. (2006): *Microchannel flow control through a combined electromagnetohydrodynamic transport*.– J. Phys. D-Appl. Phys., vol.39, No.24, pp.53-64.

[8] Sarkar S and Ganguly S. (2015): *Fully developed thermal transport in combined pressure and electroosmotically driven flow of nanofluid in a microchannel under the effect of a magnetic field*.– Microfluid and Nanofluid, vol.18, pp.623-36.

[9] Buren M., Jian Y.J. and Chang L. (2014*): Electromagnetohydrodynamic flow through a microparallel channel with corrugated walls*.– J. Phys. D-Appl. Phys., vol.47, No.42, pp.5501.

[10] Moghaddam S. (2013): *MHD micropumping of power-law fluids: a numerical solution*.– Korea-Aust. Rheol., vol.25, pp.29-37.

[11] Xie Z.Y. and Jian Y.J. (2017): *Rotating electromagnetohydrodynamic flow of power-law fluids through a microparallel channel*.– Colloid Surf. A-Physicochem. Eng. Asp., vol.529, pp.334-45.

[12] Gravesen P., Branebjerg J. and Jensen O.S. (1993): *Microfludics-a review*.– J. Micromech and Microeng, vol.3, pp.168-182.

[13] Yang C., Ooi K., Wong T. and Masliyah J.H. (2004): *Frequency-dependent laminar electroosmotic flow in a closed-end rectangular microchannel*.– J. Colloid and Interface Sci., vol.275, No.2, pp.679-698.

[14] Luo W.J., Pan Y.J. and Yang R.J. (2004): *Transient analysis of electro-osmotic secondary flow induced by dc or ac electric field in a curved rectangular microchannel*.– J. Micromech. Microeng., vol.5, pp.463-473.

[15] Liu Q., Jian Y., and Yang L. (2011): *Time periodic electroosmotic flow of Maxwell fluids between two micro-parallel plates*.– J. Non-Newtonian Mech., vol.166, No.9-10, pp.478-486.

[16] Oni M.O and Jha B.K. (2020): *Electroosmotic natural convection flow in a vertical microchannel with asymmetric heat fluxes*.– A Springer Nature Journal, https://doi.org/10.1007/s42452-020-03413-7.

[17] Ghosal S. (2004): *Fluid mechanics of electroosmotic flow and its effect on band boarding in capillary electrophroresis*.– Electrophoresis, vol.25, No.2, pp.214-228.

[18] Xuan X. (2008): *Joule heating in electrokinetic flow*.– Electrophoresis, vol.29, No.1, pp.33-43.

[19] Wang X., Qiao Y., Qi H. and Xu H. (2021): *Effect of magnetic field on electroosmotic flow of viscoelastic fluids in a microchannel*.– Electrophoresis, vol.42, No.21-22, pp.2347-2355.

[20] Yang J. and Kwok D.Y. (2004): *Analytical treatment of electrokinetic microfluidics in hydrophobic microchannels*.– Anal. Chim. Acta., vol.507, No.1, pp.39-53.

[21] Kang Y., Ooi K.T., Yang C. and Wong T.N. (2005): *Frequency-dependent velocity and vorticity fields of electro-osmotic flow in a closed-end cylindrical microchannel*.– J. Micromech and Microeng., vol.15, pp.301-312.

[22] Jayaraj S., Kang S. and Suh Y.K. (2007): *A review on the analysis and experiment of fluid flow and mixing in micro-channels*.– J. Mech. Sci. Technol., vol.21, pp.536-548.

[23] Chakraborty S. and Paul D. (2006): *Microchannel flow control through a combined electro-magneto-hydro-dynamic transport*.– J. Phys. D. Appl. Phys., vol.39, No.24, pp.5364-5371.

[24] Jang J. and Lee S.S. (2000): *Theoretical and experimental study of MHD (magnetohydrodynamic) micropump*.– Sens. Actuators A Phys., vol.80, No.1, pp.84-89

[25] Jian Y., Si D., Chang L. and Liu Q. (2015): *Transient rotating electromagnetohydrodynamic micropumps between two infinite microparallel plates*.– Chem. Eng. Sci., vol.134, pp.12-22.

[26] Ganguly S., Sarkar S., Hota T.K. and Mishra M. (2015): *Thermally developing combined electroosmotic and pressure-driven flow of in a microchannel under the effect of magnetic field*.– Chem. Eng. Sci.,vol.126, pp.10-21.

[27] Mirza I.A., Abdulhameed M., Vieru D. and Shafie S. (2016): *Transient electro-magneto-hydrodynamic two-phase blood flow and thermal transport through a capillary vessel*.– Comput. Methods Programs Biomed., vol.137, pp.149-166.

[28] Tso C.P. and Sundaravadivelu K. (2001): *Capillary flow between parallel plates in the presence of an electromagnetic field*.– J. Phys. D Appl Phys., vol.34, pp.3522-3527.

[29] Duwairi H. and Abdullah M. (2006): *Thermal and flow analysis of a magneto-hydrodynamic micropump*.– Microsyst. Technol., vol.13, pp.33-39.

[30] Shit G.C., Mondal A., Sinha A. and Kundu P.K (2016): *Electro-osmotically driven MHD flow and heat transfer in micro-channel*.– Phys. A Stat. Mech. Its. Appl., vol.449, pp.437-454.

[31] Kiyasatfar M. and Pourmahmoud N. (2016): *Laminar MHD flow and heat transfer of power-law fluids in square microchannels*.– Int. J. Therm. Sci., vol.99, pp.26-35.

[32] Liu Y., Jian Y. and Tan W. (2018): *Entropy generation of electromagnetohydrodynamic (EMHD) flow in a curved rectangular microchannel*.– Int. J. Heat Mass Transf., vol.127, pp.901-913.

[33] Mondal A., Mandal P.K., Weigand B. and Nayak A.K. (2020): *Entropic and heat-transfer analysis of EMHD flows with temperaturedependent properties*.– Fluid Dyn. Res.,vol.52, No.6, pp.065503.

[34] Sheikholeslami M. and Ganji D.D. (2016): *Nanofluid hydrothermal behavior in existence of Lorentz forces considering Joule heating effect*.– J. Mol. Liq., vol.224, pp.526-537.

[35] Dogonchi A.S. and Ganji D.D. (2016): *Thermal radiation effect on the Nano-fluid buoyancy flow and heat transfer over a stretching sheet considering Brownian motion*.– J. Mol. Liq., vol.223, pp.521-527.

[36] Mahapatra B. and Bandopadhyay A. (2021): *Numerical analysis of combined electroosmotic-pressure driven flow of a viscoelastic fluid over high zeta potential modulated surfaces*.– Phys. Fluids., vol.33, No.1. p.35.

[37] Labroopulu F., Dorrepael J.M. and Chandna O.P. (1996): *Oblique flow impinging on a wall with suction or blowing*.– Acta Mech., vol.115, pp.15-25.

[38] Attia A. (2010): *The effect of suction and injection on unsteady Couette flow with variable properties*.– Kragujevac J Sci., vol.32, pp.17-24.

[39] Ahmed S. and Khatun H. (2013): *Magnetohydrodynamic oscillatory flow in a planer porous channel with suction and injection*.– Int. J. Eng. Res. Techno., vol.2, No.11, pp.1024-1029.

[40] Magyari E. and Chamkha A.J. (2010): *Combined effect of heat generation or absorption and first-order chemical reaction on micropolar fluid flows over a uniformly stretched permeable surface: the full analytical solution*.– Int. J. Therm. Sci., vol.49, No.9, pp.1821-1828.

[41] Rundora L. and Makinde O.D. (2013): *Effect of suction/injection on unsteady reactive variable viscosity non-Newtonian fluid flow in a channel filled with porous medium and convective boundary conditions*.– J. Petrol. Sci. Eng., vol.108, pp.328-335.

[42] Hamid R.A., Arifin MdN. and Nazar R. (2013): *Effect of radiation Joule heating and viscous dissipation on MHD Marangoni convection over a flat surface with suction and injection*.– World Appl. Sci. J., vol.21, pp.933-938.

[43] Ghasemi S.E., Hatami M. and Ahangar G.H.R.M. (2014): *Electrohydrodynamic flow analysis in a circular cylindrical conduit using least square method*.– J. Electrostat., vol.72, No.1, pp.47-52.

[44] Ravindran R. and Ganpathirao M. (2013): *Non-uniform slot suction/injection into mixed convection boundary layer flow over vertical cone*.– Appl. Math. Mech., vol.34, pp.1327-38.

[45] Kundu B. and Saha S. (2022): *Review and analysis of electro-magnetohydrodynamic flow and heat transport in microchannels*.– Energies, pp.21-24.

[46] Jha B.K. and Apere C.A. (2010): *Unsteady MHD Couette flow in an annuli: the Riemann-sum approximation approach*.– J. Phy. Soc. Jpn., vol.79, No.12, pp.124403-124408.

[47] Jha B.K and Oni M.O. (2018): *An analytical solution for temperature field around a cylindrical surface subjected to a time dependent heat flux: an alternative approach*.– Alexandr. Eng. J., vol.57, No.2, pp.927-929.

[48] Khadrawi A.F. and Al-Nimr M.A. (2007): *Unsteady natural convection fluid flow in a vertical microchannel under the effect of the dual-phase-lag heat conduction model*.– Int. J. Thermophys, vol.28, pp.1387-1400.

[49] Tzou D.Y. (1995): *A unified field approach for heat conduction from macro- to micro-scales*.– J. Heat Transfer, vol.117, No.2, pp.8-16.

Received: July16, 2023
Revised: September 28, 2023